IOPscience

Home   Search   Collections   Journals   About   Contact us   My IOPscience

Energy harvesting from a DE-based dynamic vibro-impact system

Energy harvesting from a DE-based dynamic vibro-impact system

D. Yurchenko[1], D. V. Val[2], Z. H. Lai[1,3], G. Gu[2], G. Thomson[1]

[1]IMPEE, Heriot-Watt University, Edinburgh, UK

[2]Institute for Infrastructure & Environment, Heriot-Watt University, Edinburgh, UK

[3]School of Mechatronics Engineering, Nanchang University, Nanchang, 330031, People's Republic of China

E-mail: laizh@ncu.edu.cn

Abstract. Dielectric elastomer (DE) generators may be used in harvesting energy from ambient vibrations. Based on existing research on the mechanical properties of a circular DE membrane, a DE-based dynamic vibro-impact system is proposed in this paper to convert vibrational energy into electrical one. The dimensional, electrical and dynamic parameters of the DE membrane are analysed and then used to numerically estimate the output voltage of the proposed system. The system output performances under harmonic excitation are further discussed. At last, the comparison study has been conducted with an electromagnetic energy harvesting system, served as a "shaking" flashlight.

1. Introduction

Vibrational energy recovered from various sources of ambient vibrations is considered to be renewable, clean and can be converted into electrical energy. The majority of investigations on energy harvesting (EH) from ambient vibrations so far have been focused on the use of piezoelectric (PZT) materials [1-3]. These PZT EH devices have simple structures and relatively high energy conversion efficiency. However, these devices have certain limitations and shortcomings and are less versatile than desired [4], which greatly restricts their areas of application and generates small amount of energy, usually in the range of tens to hundreds of mW.

In recent years, dielectric elastomers (DEs) have shown their advantages for a vibrational energy conversion and attracted much attention from researchers [5-10]. Compared with PZT materials, DEs can convert linear or rotational motion under a wide frequency range [11]. Dielectric elastomer generators have also been developed for both small-scale energy scavenging and large-scale energy generation. The latter ones, which are of a regular or "mm/cm" scale, can potentially be useful for charging small devices or wearable sensors. DE is a type of electro-active polymers such as acrylic, silicones, polyurethanes, fluoroelastomers, ethylene-propylene rubbers, etc. It possesses such advantages as a low mass density, large deformability, high energy density, rather good electro-mechanical conversion efficiency, moderate or low cost, solid-state monolithic embodiment with no sliding parts, good chemical resistance to corrosive environments, silent operation, as well as easy for manufacturing and recycling [12].

DE acts as a deformable capacitor in the vibrational energy conversion. A DE generator was first proposed by Pelrine et al. back in 2001 [13]. Suo et al. [14] established the DE theory based on thermodynamics and continuum mechanics. Following their work, a lot of research results related to DE generators have been published. The basic material properties, failure mechanisms and identification methods were studied [15-17]. A detailed model that describes the four cycling phases of DE-based energy harvesting was developed in [18], whereas the influence of the material dielectric coefficient on the energy harvesting performance and bias voltage were reported in [19]. These researches laid the foundation for further investigations in DE-based energy harvesting systems. Up to now, several DE-based energy harvesting devices have been developed, e.g. an ocean wave generator [20-22]. These researches emphasized that a major advantage of DE-based generators was their high energy density of more than 0.4 J/g [23], especially at a low frequency and high stretch area.

The majority of publications on DE generators provide some theoretical analysis, whereas only a few works have studied the practical vibrational energy conversion of a DE generator and its performance, which limits the application of DE for vibrational energy harvesting in real life. Therefore, some specific devices based on DE should be further considered, with analyses of energy conversion and evaluation of EH performance according to ambient vibration.

In this paper, in order to practically utilize DE to convert vibrational energy into electrical energy, a DE-based dynamic vibro-impact system [24-26] under external excitation is proposed. The design of the system is inspired by the research results that vibro-impact motion makes the system dynamics highly nonlinear but in some cases this effect may lead to more efficient energy harvesting. The idea of using a vibro-impacting motion for energy harvesting has relatively recently been reported in [27], where the energy harvesting frequency range of 29~41 Hz was achieved. Lately, a number of papers have proposed various designs of EH devices with rigid barriers [28-34]. It is promising to propose a novel DE-based vibro-impact EH system by considering these PZT-based vibro-impact EH systems.

The DE-based vibrational energy harvesting in a vibro-impact system is based on the capacitance changes resulting from the deformation of DE under an external excitation. To develop such an energy harvesting system, one needs to estimate how much energy will be harvested. To access that a parametric study of a DE generator, which takes into account its dynamic behaviour and mechanical properties of the DE material, is necessary.

This paper discusses the basic electrical and mechanical properties of a DE material in Section 2. Dynamic model of the proposed DE EH device, its features and basic principles are discussed in Section 3. Numerical simulations of various parameters of the system are presented in Section 4. In Section 5, the influences of the parameters of the excitation are studied, along with a comparison with an electromagnetic energy harvesting system.

2. Material properties of DE

2.1. Basic principle of DE

A DE-based generator consists of a thin elastomer layer (membrane) between two electrodes. The principle of power generation by a DE generator relies on increased electrical potential due to mechanical deformation of the elastomer. The capacitance of a DE is

$$C = \frac{\varepsilon_0 \varepsilon_r A_{DE}}{h} = \frac{\varepsilon_0 \varepsilon_r V}{h^2} \tag{1}$$

where ε_0 is the vacuum permittivity, ε_r is the relative permittivity of the DE, A_{DE} is the effective area (coated on each side by electrodes), h and V are the thickness and volume of the elastomer, respectively. The second equality in (1) can be written because the volume of elastomer is essentially a constant due to the elastomer incompressibility, i.e., $A_{DE}h = V = \text{constant}$.

Another important formula used here relates the charge Q on the membrane and voltage U: $Q=CU$. Two different regimes are possible to observe with variable capacitance: constant charge and constant voltage. The first implies an increase in voltage with a decrease in capacitance; the second indicates a decrease in charge with a decrease in capacitance. However, the constant charge regime is less feasible because it requires disconnecting the power supply periodically and frequently, which is difficult in implementation and questionable from reliability point of view. Thus, this paper is focused on the constant voltage case. The fact that the DE devices require some initial voltage is considered against them but the amount of recovered energy is proportional to the initial voltage and, therefore, such devices can generate significantly larger amount of energy than PZT devices of similar size.

Suppose that a DE membrane undergoes a mechanical deformation that causes an increase in the effective area and reduction of its thickness, as shown in Figure 1(a). Therefore, the deformed DE membrane has an increased capacitance according to (1). The deformed DE membrane is then charged from an electrical power source. The minor deformation due to electroelastic pressure can be neglected because it is relatively small compared with the total deformation of the DE membrane. As the mechanical force causing the deformation is removed (i.e., as the DE volume is restored, as shown in Figure 1(b)), the electrical potential and output voltage between the electrode layers increase due to the decreasing capacitance of the DE membrane. Therefore, charges with elevated electrical potential can be used for energy harvesting.
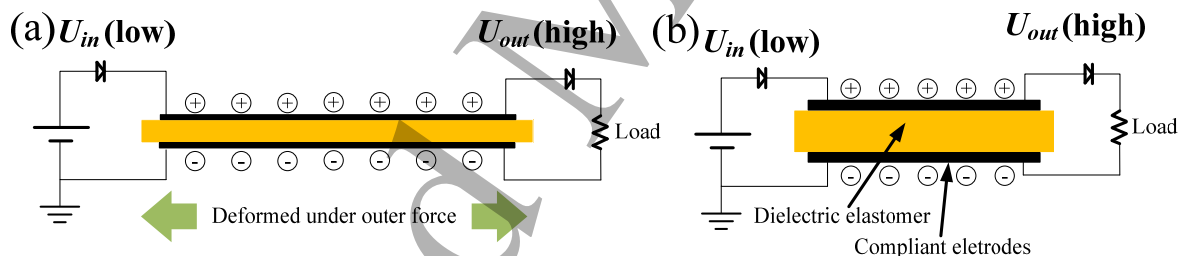

Figure 1. Operating principle of a DE-based energy generator.

2.2. Mechanical properties of DE

In order to obtain the output voltage and electrical energy generated from a deformed DE, it is of great importance to exactly describe the deformation condition of a DE under an external force. In this paper, a pre-stretched circular DE membrane under impact of a fast moving spherical ball in its centre is considered, as shown in Figure 2. The original radius and thickness of the DE membrane before stretching are R_1 and h_1, respectively. The membrane is λ-th times pre-stretched in its radial direction, thus its radius and thickness become $R_2 = \lambda R_1$ and $h_2 = h_1 / \lambda^2$, respectively. A spherical ball with radius r_b is then used to mechanically deform the membrane in the out-of-plane direction. The deflection of the membrane caused by the ball impact is denoted as x, and the force on the ball exerted by the membrane is denoted as $f(x)$, as shown in Figure 2(b).
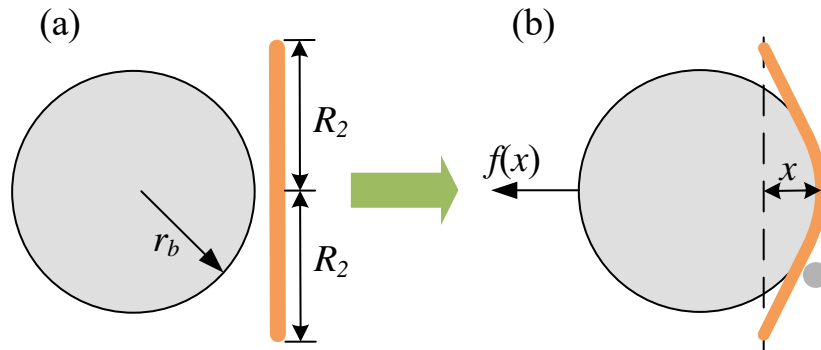
Figure 2. The shapes of DE membrane (a) before and (b) after pressed by a spherical ball.

The relation between $f(x)$ and x is the key to calculate the capacitance of the DE membrane under deformation resulting from the external excitation, which will be introduced in Section 3. In this subsection, this relation is obtained through experiments.

A DE material named VHB^{TM} 4910 (3M Corporation) is used in the experiments mentioned in this paper. A circular membrane with radius $R_1 = 3.15$ mm and thickness $h_1 = 1$ mm was pre-stretched radially twice of its size, namely $R_2 = 6.3$ mm and $h_2 = 0.25$ mm. This membrane was then fixed by two identical cylindrical frames, whose inner radius $R_{cin} = 6.3$ mm, as shown in Figure 3(a). The relation between the force on the ball and the deflection of the DE membrane was measured using an Instron 5567 material test system, as shown in Figure 3(b).
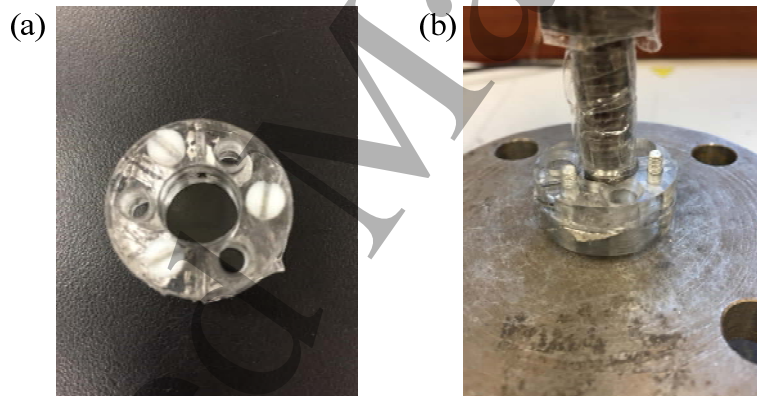
Figure 3. Picture of (a) pre-stretched DE membrane and (b) the experiment.

The data from three experiments are shown in Figure 4. For further calculation, the data are fitted by the following exponential function:

$$f(x) = K \cdot x^n \tag{2}$$

where $K = 4.0847 \times 10^5$, $n = 2.6$ and $f(x)$ in N. It can be seen from Figure 4, the fitted curve is in a good agreement with the experimental data. Therefore, (2) is used for further calculations in this paper. The reason for noisy experimental data comes from the fact that very low values of the force used to load the membrane. Although the noise looks significant its values are mainly within ±0.2 N, which in absolute terms are very small. It can also be seen that the noise decreases as the force increases.

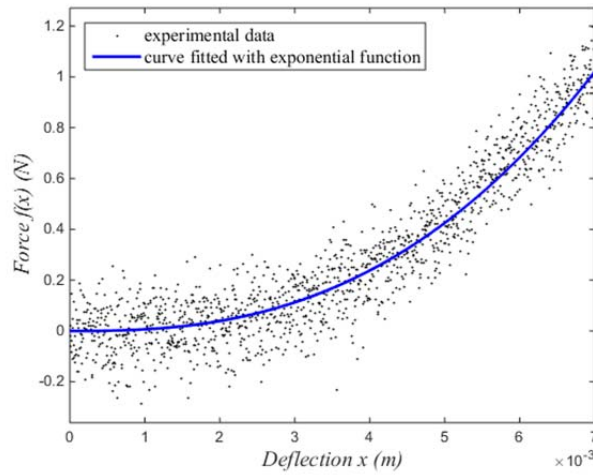Figure 4. Experimental data and fitted curve of the relation between force and deflection.

3. Modelling and analysis

3.1. Model introduction

A dynamic vibro-impact model presented in this paper for energy harvesting from vibrations is shown in Figure 5. The system comprises a cylinder, an inner ball sliding freely in inside the cylinder and two pre-stretched DE membranes at both ends of the cylinder. Both pre-stretched membranes are sandwiched between compliant electrodes and wires are connected to both sides of each membrane. Each membrane is fixed between two identical cylindrical frames and then connected to the cylinder. The system can move freely in the horizontal direction subject to an external excitation.
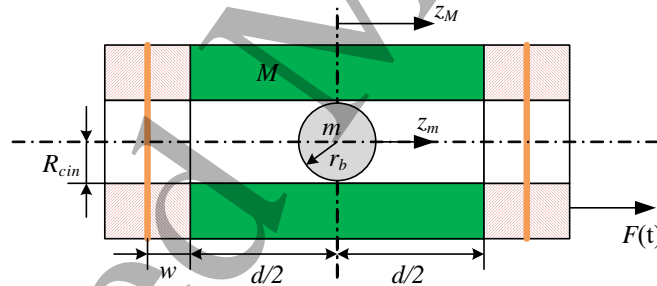

Figure 5. Sketch of the proposed DE-based dynamic vibro-impact system.

In this model, the mass of the outer structure (the system without the inner ball) is denoted by M and the mass of the inner ball by m. The inner radiuses of the cylinder is R_{cin}, the radius of the ball is r_b. The length of the cylinder is d whereas the width of the cylindrical frame is denoted by w. The cylinder is excited by an external force $F(t)$ applied along the horizontal direction. Here, z_M and z_m are defined as the displacements in the horizontal direction of the outer structure and inner ball, respectively, as shown in Figure 5. The origin of the coordinate system for the inner ball coincides with that of the cylinder and is set in the middle of the cylinder. The friction between the ball and slot is quite small and ignored.

The device is meant to work in the following way. When the cylinder moves under the external excitation the ball moves freely inside of it until it collides against one of the membranes causing its deformation. At the maximum deformation the membrane capacitance will be maximal

(corresponding to its minimal thickness due to deformation). This will lead to an increase in charge, which is being harvested at that moment, thereby converting mechanical energy into electric. Then the ball velocity changes to opposite (refers to the cylinder) and it moves until it hits either membranes again, and the process will repeat itself again and again. Obviously, to generate more energy larger deformations of the membranes are required, which can be achieved by using the internal ball with bigger mass and higher impacting velocity. The latter depends on the type of a steady-state motion as well as the membrane mechanical properties.

3.2. Parametric analysis of the system

It is important to understand how the DE membrane works and thus its electrical properties are revisited here. The DE membrane has four stages in this model, as shown in Figure 6(a). Initial stage 1 represents the original condition of the circular membrane with radius R_1 and thickness h_1. Stage 2 indicates the initial condition of the membrane after being stretched to radius $R_2 = R_{cin}$. Stage 3 shows the largest deformation condition of the membrane at impacts. The membrane will recover its shape at stage 4 after an impact so that its shape is the same as at stage 2 but its electrical properties are not. Stages 2~4 will be repeated in each cycle of the external excitation.
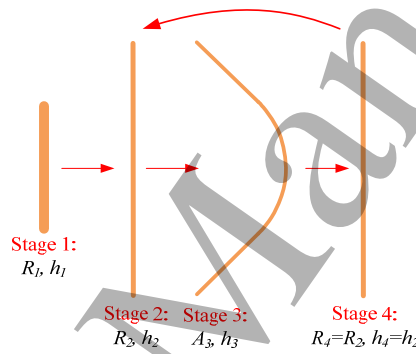

Figure 6. Shapes of the DE membrane at different stages.

In this paper, R_i, A_i, h_i, C_i, U_{DEi} and Q_i ($i = 1, 2, 3, 4$) are used to represent the radius, area, thickness, capacitance, voltage and charge of the membrane at each stage, respectively. Denote $V = A_i h_i$ as the constant volume of the membrane. Input voltage U_{in} is applied to the membrane at stages 2, 3 and 4. The dimensional and electrical parameters of the membrane at different stages [6] are summarized in Table 1.

Table 1. Dimensional parameters and electrical parameters of the DE membrane at different stages.

Stage	Dimensional parameters			Electrical parameters		
	Radius	Area	Thickness	Capacitance	Voltage	Charge
Stage 1	R_1	$A_1 = \pi R_1^2$	h_1	C_1	$U_{DE1} = 0$	$Q_1 = 0$
Stage 2	$R_2 = R_{cin}$	$A_2 = \pi R_2^2$	$h_2 = V / A_2$	$C_2 = \dfrac{\varepsilon_0 \varepsilon_r V}{h_2^2}$	$U_{DE2} = U_{in}$	$Q_2 = C_2 U_{DE2}$
Stage 3	--	A_3	$h_3 = V / A_3$	$C_3 = \dfrac{\varepsilon_0 \varepsilon_r V}{h_3^2}$	$U_{DE3} = U_{in}$	$Q_3 = C_3 U_{DE3}$
Stage 4	$R_4 = R_2$	$A_4 = A_2$	$h_4 = h_2$	$C_4 = C_2$	$U_{DE4} = Q_4 / C_4$	$Q_4 = Q_3$

The original dimensional parameters of the membrane are given at stage 1. At stage 2, the membrane is pre-stretched to a new radius R_2, which determines the new thickness h_2 and the initial capacitance C_2 of the membrane. At stage 3, the membrane is under impact from the inner ball. As shown in Figure 7, the membrane can be treated as consisting of two parts. The part shown by a solid line adheres to the ball, hence, its area is the same as the surface area of the contact part of the ball, denoted as A_{31}. The part shown by a dashed line, whose area is A_{32}, is tangential to the ball and has an angle of α to the original membrane plane. Therefore, the area of the membrane at stage 3 is:

$$A_3 = A_{31} + A_{32} \tag{3}$$

where the first component corresponds to the surface area of a spherical segment, whereas the second component is the surface area of a cone segment. It can be calculated according to Figure 7 that:

$$\begin{cases} A_{31} = 2\pi r_b (r_b - r_b \cos\alpha) = 2\pi r_b^2 (1 - \cos\alpha) \\ A_{32} = \dfrac{\pi R_2^2 - \pi (r \sin\alpha)^2}{\cos\alpha} \end{cases} \tag{4}$$
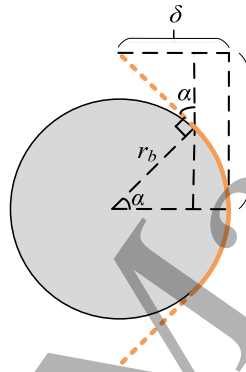

Figure 7. Geometry of the DE membrane at largest deformation condition.

In (4), all the parameters are given except of the angle α, which is determined by the interaction of the inner ball and the membrane. If δ denotes the largest deflection of the membrane at an impact, the relation between α and δ can be written as:

$$\tan\alpha = \frac{\sin\alpha}{\cos\alpha} = \frac{\delta - r_b(1 - \cos\alpha)}{R_2 - r_b \sin\alpha} \tag{5}$$

Taking into account the trigonometric identity $\sin^2\alpha + \cos^2\alpha = 1$, the value of α can be obtained as following equation:

$$\cos\alpha = \frac{-2r_b(\delta - r_b) + 2R_2\sqrt{R_2^2 + \delta^2 - 2\delta r_b}}{2\left[R_2^2 + (\delta - r_b)^2\right]} \tag{6}$$

Therefore, having known the value of δ, the value of α and then the area of the membrane at stage 3 can be calculated. The area A_3, thickness h_3 and capacitance C_3 of the membrane at this stage can be obtained as well. The value of δ depends on the dynamic behaviours of the cylinder and inner ball, which are governed by their relative motion/position and impact interaction. Therefore, it is important to further conduct the dynamic analysis of the system.

Suppose a harmonic excitation $F(t) = A\cos(2\pi f_0 t)$ is applied to the system, where A and f_0 denote its amplitude and frequency, respectively. Due to the low mass ratio of the inner ball to the

outer structure, impacts have little effect on the outer structure. The outer structure will move under this excitation as following:

$$z_M{''}(t)=F(t)/M \tag{7}$$

The inner ball, in its turn, experiences no external force (friction has been neglected), which means its velocities will not change until the ball impacts the membrane. Introducing the relative displacement $\Delta z = z_M - z_m$ as the difference between z_M and z_m, and $s = d + 2w - 2r_b$ the largest distance of the ball moving inside the cylinder. Thus, the conditions of impacts can be written as:

$$|\Delta z| = |z_M - z_m| = s/2 \tag{8}$$

The velocity of the ball changes after impacts. Let v_{m-} and v_{m+} represent the velocities of the ball before and after each impact, and v_{M-} and v_{M+} the velocities of the outer structure before and after each impact, respectively. Here, $v_{M-} = v_{M+} = v_M$ due to the above assumption and application of the excitation force. When impacts occur the varying elastic force of the membrane $f(x)$ will produce negative work on the ball until it reaches the largest deflection δ, at that moment the velocity of the ball becomes equal to v_M. Considering the outer structure as the reference frame, the following equation can be written according to the kinetic energy theorem

$$0 - \frac{1}{2}m(v_{m-} - v_M)^2 = \int_0^\delta [-f(x)]dx = -\int_0^\delta Kx^n dx = -\frac{K}{n+1}\delta^{n+1} \tag{9}$$

then the largest deflection of the membrane at impacts can be obtained:

$$\delta = \left[\frac{n+1}{2K}m(v_{m-} - v_M)^2\right]^{\frac{1}{n+1}} \tag{10}$$

Substituting the value of δ into (6) leads to the value of α and, consequently, the dimensional and electrical parameters of the membrane during an impact can be found. It should be stressed that nonlinear model (2) is used in this paper for estimating the membrane deformation (10) only, which defines the voltage output of the DE element. Formula (2) implies the Hertzian contact of two bodies, which takes the following assumptions, among others, that the strain is small and the contact area is much smaller than the characteristic dimensions of the contacting bodies. Since these assumptions are not fulfilled formula (2) is not used for describing the ball dynamics at the impacts.

To estimate the ball velocity after an impact the Newton's model of impact is implemented

$$v_{m+} = -r(v_{m-} - v_{M-}) + v_{M+} = -rv_{m-} + (r+1)v_M \tag{11}$$

where r is the restitution coefficient of the membrane. The ball will keep moving at this velocity until next impact.

According to the above analysis, the displacements and velocities of the outer structure and the ball can be obtained at any time provided the external excitation of the system and initial conditions are specified. The dimensional and electrical parameters of the membrane at stage 3 can be obtained as well.

At stage 4, the dimensional parameters and capacitance of the membrane are exactly the same as those at stage 2. However, the charge on the membrane will keep at Q_3 level by the end of an impact. At this moment, the voltage across the membrane is

$$U_{DE4} = Q_4 / C_4 = \frac{C_3}{C_2} U_{in} = \frac{h_2^2}{h_3^2} U_{in} \tag{12}$$

Obviously, $h_2 > h_3$, thus, $U_{DE4} > U_{in}$. This indicates that impacts between the ball and membrane will produce higher output voltage, as expected. Therefore, the external vibrational energy can be converted to electric energy through the ball's impacts by using the presented dynamic model.

4. Simulated results

4.1. Energy harvesting circuit

In order to harvest the electrical energy produced by the DE-based dynamic vibro-impact system, the DE membranes are connected in parallel to an electrical circuit for energy harvesting as illustrated in Figure 8(a). The circuit controls the charge on the DE membranes through an energy harvesting cycle that has been previously studied both theoretically and experimentally in [9,23]. The system transfers charges from a voltage supply (U_{in}) up to a higher voltage (U_{out}) when the energy is supplied to a load. Thus, the proposed system provides a gain in electrical energy. In the circuit shown in Figure 8(a), the diode only allows the charging current to flow when the voltage of both DE membranes is lower than that of the power supply (U_{in}). The Zener diode with a breakdown voltage U_z allows the charge to flow from the DE membranes to the load when the voltage of either membranes is larger than U_z. Thus, the diode and Zener act as switches, turning on and off automatically depending on the voltage of the DE membranes. In this circuit, $U_{in} \leq U_z$ should be satisfied and their values need to be carefully chosen because they control the charge state of the system.

According to the analysis of the circuit, when $U_z = U_{in}$, the output voltage of the system and the charges of the membranes can be obtained ideally, as shown in Figure 8(b). At stage 2, $U_{out} = U_{in}$, $Q_2 = C_2 U_{in}$. When one of the membranes is stretched under impact and changed to stage 3, the capacitance of the membrane increases and the voltage supply charges to the membrane until $Q_3 = C_3 U_{in}$. The voltage of the membrane increases up to U_{DE4} in its recovery to stage 4. The charges then flow from the membrane to the load, with output voltage U_{out} decreasing according to $Q=C_2 U$ until the voltage of the membrane drops to U_{in} again and the extra charges of the membrane are fully released. It can be seen that the charges and voltages of either membranes at different stages in this cycle conform to our previous analyses in Talbe 1.
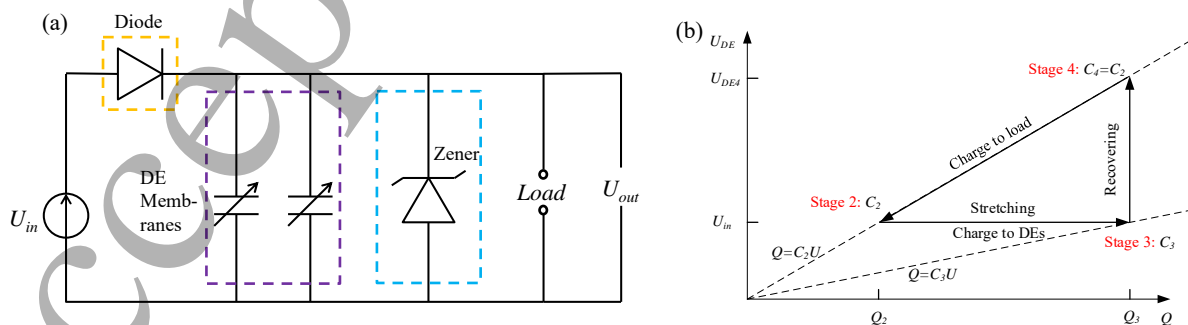

Figure 8. (a) Energy harvesting circuit and (b) schematics showing one energy harvesting cycle.

It can be seen that in one complete cycle, $\Delta Q = Q_3 - Q_2$ is boosted from the low input voltage U_{in} to high output voltage U_{impact} :

$$W = \frac{1}{2} U_{in}^2 \left(C_3 - C_2 \right) \qquad (13)$$

In this paper, the electrical parameters in the circuit are set at $U_{in} = U_z = 2000$ V.

4.2. Simulation

It is difficult to obtain the system response analytically due to its high nonlinear. Therefore, the 4th Runge-Kutta algorithm is adopted in this paper to solve differential equation (7). The system response can then be obtained. For a high computational accuracy, the time step in the computational process is set at 10^{-5} s in all following simulations in this paper.

Depending on the initial conditions as well as the excitation amplitude and frequency various types of motion can be observed. In this paper a number of different cases are studied under pure harmonic excitation. The following set of parameters was used for numerical simulations: $M = 124.5$ g, $m = 3.5$ g, $R_1 = 3.15$ mm, $h_1 = 1$ mm, $R_2 = R_{in} = 6.3$ mm, $r_b = 5$ mm, $d = 42$ mm, $w = 6$ mm, whereas electrical parameters of the system have been given in subsection 4.1.

In Figure 9 displacements and velocities of the cylinder (a, b) and ball (c, d) without impacts are presented to validate the code. This case was achieved by setting $A = 0.01$ N, $f_0 = 2$ Hz, $r = 1$ and the following initial conditions: $z_M(0) = -A / [M(2\pi f_0)^2]$, $z_M'(0) = 0$, $z_m(0) = 0$, $z_m'(0) = 0$. Figures 9(e, f) present the relative displacement $\Delta z = z_M - z_m$ and voltage generated during this regime. Apparently due to the low excitation amplitude the ball does not collide against either membrane and thus its displacement and velocity keep zero. Without impact no extra voltage is produced and thus Figure 9(f) shows applied voltage of 2 kV at the output.
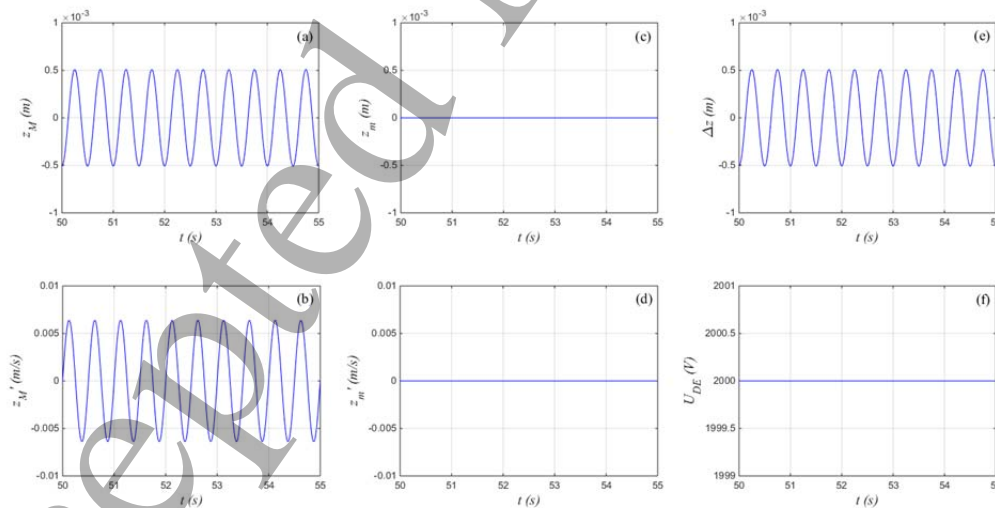

Figure 9. Displacements and velocities of the outer structure (a, b) and the ball (c, d), relative displacement and voltage (e, f) versus time for $A = 0.01$ N, $f_0 = 2$ Hz, $r = 1$.

A special case of a vibro-impact motion with two consecutive impacts against two opposite membranes within each cycle is considered next. It is not difficult to find the initial conditions for this

type of motion, which are: $z_M(0) = -A/[M(2\pi f_0)^2]$, $z_M{}'(0) = 0$, $z_m(0) = z_M(0) + s/2$ ($z_m(0) > 0$), $z_m{}'(0) = -4 f_0 z_m(0)$. Excitation amplitude and frequency have been kept the same for the purpose of comparison, i.e., A=0.01 N, $f_0 = 2$ Hz, and $r = 1$. Results of numerical simulations for this case are presented in Figure 10. As in the previous plot, Figures 10 (a, b) and (c, d) show the results of the displacements and velocities of the cylinder and ball correspondingly. In Figure 10(b) one can clearly observe "pure" or "classical" vibro-impacting regime with consequent impacts that reflects in the sharp peaks and troughs. Since this curve looks like a saw-tooth signal, it will be referred later as the saw-tooth case. Figures 10(e, f) demonstrate the relative displacement and voltage generated in this case. Another characteristic feature of this response is equal voltage peaks of both membranes, which are seen in Figure 10(f).
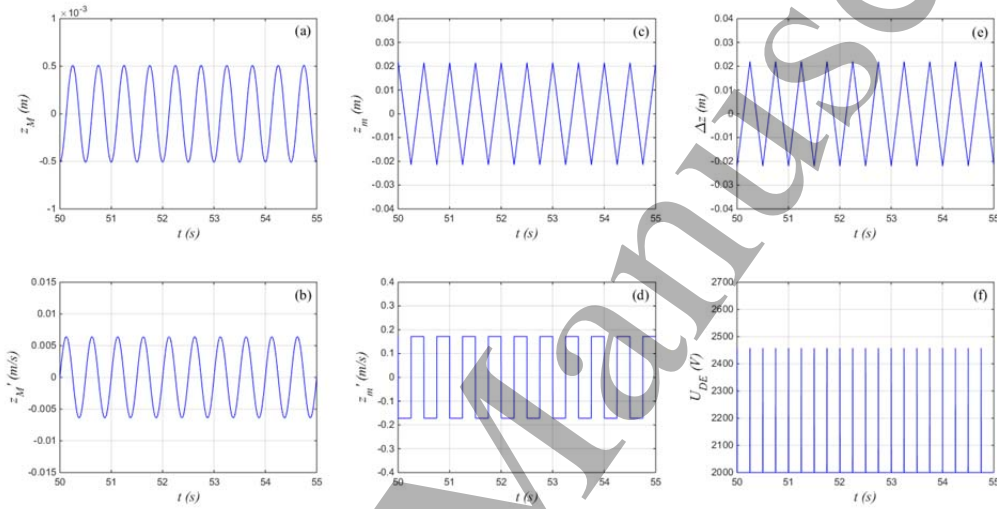

Figure 10. Displacements and velocities of the outer structure (a, b) and the ball (c, d), relative displacement and voltage (e, f) versus time for the saw-tooth case with A=0.01 N, $f_0 = 2$ Hz, $r = 1$.

Unfortunately, the above saw-tooth pattern can be easily destroyed when the excitation amplitude $A > M(2\pi f_0)^2 s/2$=0.4325. Thus, the next set of plots demonstrates results of numerical simulation for A=0.5 and all other parameters being kept the same as in Figure 10. Figures 11 (a, c) present the result for the displacements of the cylinder and ball. Apparently, this vibro-impact motion cannot be considered as classical one since two consequent impacts, occurring against the opposite membranes, may happen over a much shorter distance (see red circles in Figure 11c) than in a classical vibroimpact motion. In Figure 11(f) one can observe harvested voltage and it has low and high peaks due to low and high impact velocities that cause the membranes deformations.
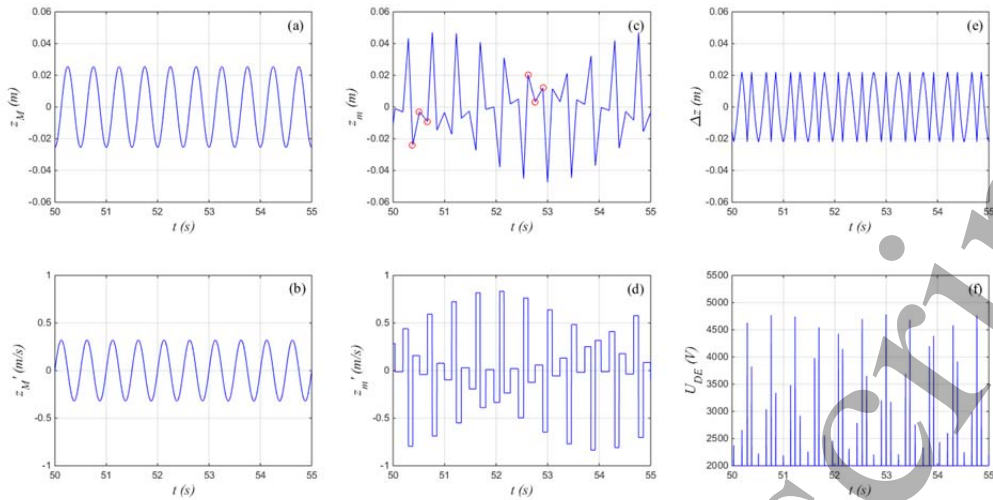
Figure 11. Displacements and velocities of the outer structure (a, b) and the ball (b, d), relative displacement and voltage (e, f) versus time for the saw-tooth case but A=0.5 N.

Another set of plots is presented in Figure 12, which corresponds to the following initial conditions: $z_M(0) = -A/[M(2\pi f_0)^2]$, $z_M'(0) = 0$, $z_m(0) = 0$, $z_m'(0) = 0$. Once again, irregular vibro-impact motion is observed in Figure 12(c), which can also be seen in Figure 12(e), where the relative difference in the displacement is plotted. This irregular motion is not similar to the one in Figure 11 because it looks like the ball hits one of the membranes twice (see red circles) before moving to the opposite membrane.
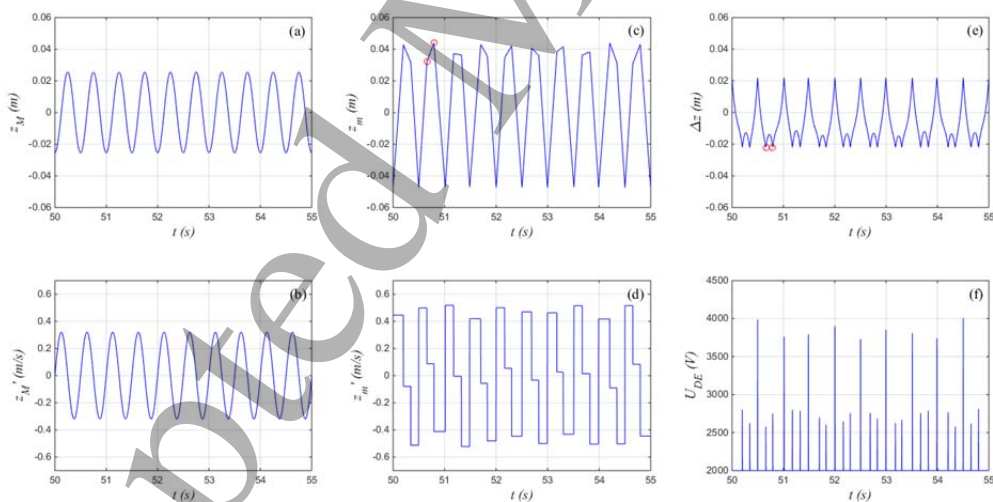

Figure 12. Displacements and velocities of the outer structure (a, b) and the ball (c, d), relative displacement and voltage (e, f) versus time for A=0.5 N, $f_0 = 2$ Hz, $r = 1$ and another set of initial conditions.

Unfortunately, it is impossible to set specific initial conditions in a real life application, especially for the ball which is inside the cylinder and cannot be controlled. Thus, it may be reasonable to assume zero initial conditions for it and the cylinder ($z_M(0) = 0$, $z_M'(0) = 0$, $z_m(0) = 0$, $z_m'(0) = 0$).

Results of this simulation for $A=0.5$, $f_0 = 2$, $r=1$ are shown in Figure 13, where the motion looks like almost chaotic.

Figure 13. Displacements and velocities of the outer structure (a, b) and the ball (c, d), relative displacement and voltage (e, f) versus time for $A=0.5$ N, $f_0 = 2$ Hz, $r=1$ and zero initial conditions.

It is of interest to understand the behaviour of the system with inelastic impact ($r<1$). In the case of the saw-tooth regime and $r=0.6$ and $r=0.3$, the results are presented in Figure 14 and 15, respectively. An asymmetric response of the ball can be observed in these two cases, which are reflected in the asymmetry of the relative displacements (see Figure 14(e) and 15(e)) and high and low periodic peaks in gained voltage.

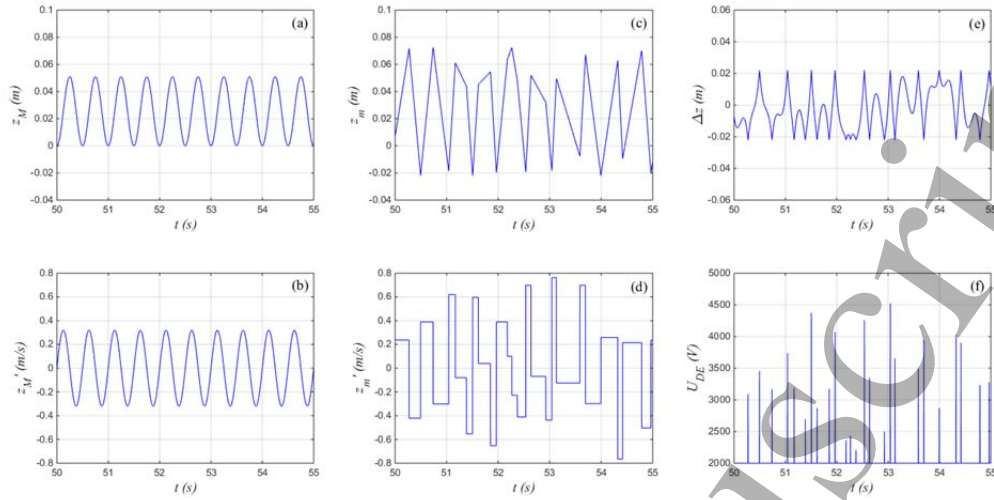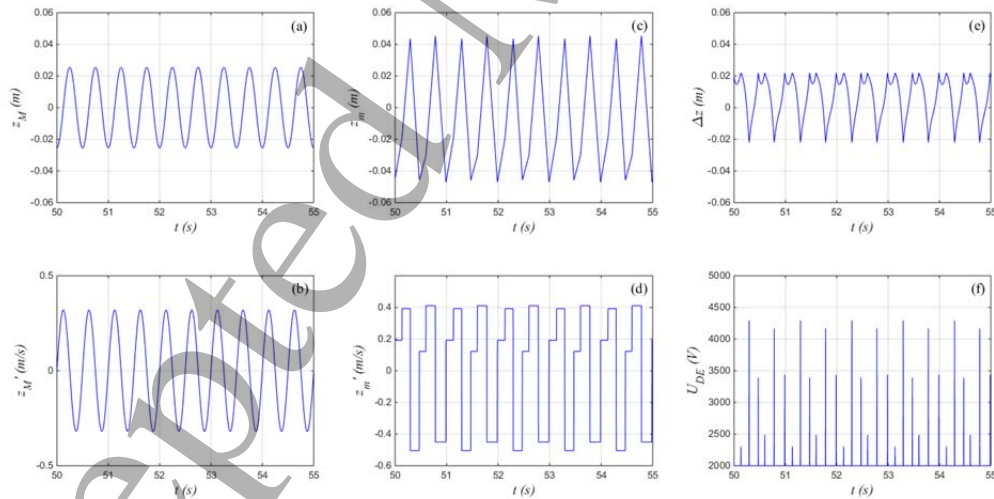Figure 14. Displacements and velocities of the outer structure (a, b) and the ball (c, d), relative displacement and voltage (e, f) versus time for the saw-tooth case with $A=0.5$ N, $f_0 = 2$ Hz, $r=0.6$.
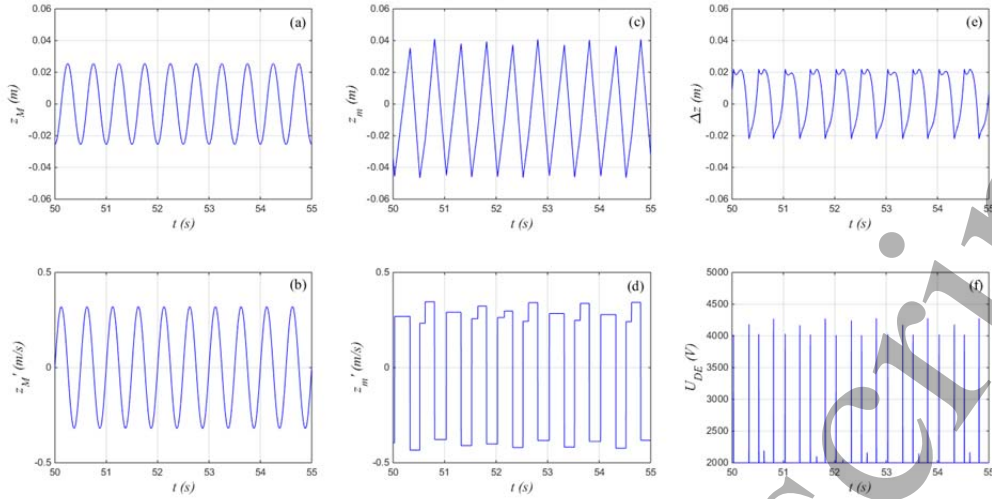
Figure 15. Displacements and velocities of the outer structure (a, b) and the ball (c, d), relative displacement and voltage (e, f) versus time for the saw-tooth case with $A=0.5$ N, $f_0 = 2$ Hz, $r=0.3$.

It should be stressed that various initial conditions led to different type of the ball response in the case of the elastic impact, as has been reported above. However, numerous numerical simulations have shown that for the inelastic impact the difference in the response type due to different initial conditions becomes almost invisible, which typically resulted in very similar patterns of harvested voltage, where a high peak is followed by a moderate peak and then a very small one.

5. Discussion

Since this paper is focused on the energy harvesting investigation, it is of primary importance to estimate the harvested electrical power. During a steady state response ($50 < t < 100$ s in this paper), the power gain of the proposed device can be obtained according to (13)

$$P = \sum_{i=1}^{N} W_i / T = \sum_{i=1}^{N} \frac{1}{2} U_{in}^2 \left(C_{3i} - C_2 \right) / T = \sum_{i=1}^{N} \frac{1}{2} C_2 U_{in} \left(U_{DE4i} - U_{in} \right) / T \tag{14}$$

where W_i denotes the energy gain during the ith impact, C_{3i} the capacitance at stage 3 at the ith impact, and U_{DE4i} the output voltage across the deformed membrane at the ith impact. N is the number of impacts within the same time interval, and $T = 50$ s accordingly. It can be seen that the power gain can be easily calculated from the harvested voltage. Therefore, the average output voltage gain of the proposed device at a steady state is defined as:

$$\langle U \rangle_T = \sum_{i=1}^{N} \left(U_{DE4i} - U_{in} \right) / T \tag{15}$$

to estimate the system output performance.

The above simulations, except of the one shown in Figure 9, have produced gain voltage shown in Table 2. It can be seen that the amounts of $\langle U \rangle_T$ at frequency $f_0 = 2$ Hz and $r=1$ have a similar magnitude (out of all considered cases). It is also interesting to note that with a decrease of the restitution coefficient the amount of $\langle U \rangle_T$ is higher than that in all other cases with $r=1$.

Table 2. Amount of the output voltage gain over 50 s ~ 100 s.

Case studied	Figure 10	Figure 11	Figure 12	Figure 13	Figure 14	Figure 15
	A=0.01	A=0.5				
	$r=1$				$r=0.6$	$r=0.3$
$\langle U \rangle_T$ (V/s)	1831	6749	6730	6989	8079	8652

5.1. Influence of amplitude and frequency of the harmonic excitation

The responses of the system under different amplitude and frequency of a harmonic excitation are studied in this subsection. The harmonic excitation $F(t) = A\cos(2\pi f_0 t)$ applied to the system results in the response amplitude of the cylinder movement that is equal to $A/[M(2\pi f_0)^2]$. Since it is easier to work with nondimensional units, the cylinder amplitude is normalized to half the distance the ball can travel freely between impacts so that:

$$\gamma = \frac{A/\left[M(2\pi f_0)^2\right]}{s/2} \tag{16}$$

Thus, to study the response of the system as a function of γ, the value of f_0 should be kept constant (all other parameters are constants and have been given above, initial conditions are all set at zero). Based on the simulated results in Subsection 4.2, the curves of $\langle U \rangle_T$ versus γ are plotted in Figure 16(a). It can be seen that with an increase of γ and therefore A, all the curves demonstrate an increasing trend. This trend is well expected because larger values of A result in a higher relative acceleration and velocity between the outer structure and inner ball at the impacts, so that most U_{DE4} increases. Therefore, the strength of the harmonic excitation has a positive effect on the magnitudes of the electrical energy converted through this system.

Figure 16(a) also indicates that $\langle U \rangle_T$ has a larger value when the frequency f_0 is larger at a same value of γ. This is better presented in Figure 16(b), which shows $\langle U \rangle_T$ curves as a function of the excitation frequency f_0 for several different values of γ. All the curves show upward trends as f_0 increasing due to the increasing number of impacts, since for each curve γ was a constant. Therefore, the frequency of the harmonic excitation also has a positive effect on the magnitudes of the electrical energy converted through this system. In addition, electrical energy can be harvested through the proposed system under wide-range frequencies.
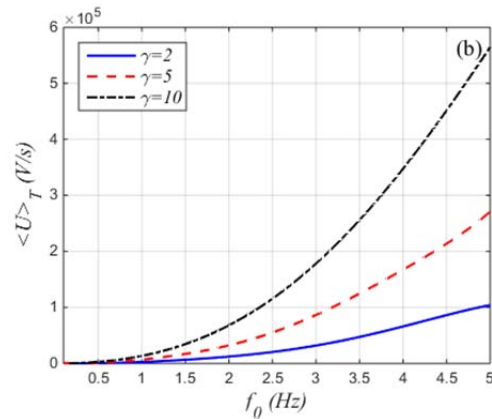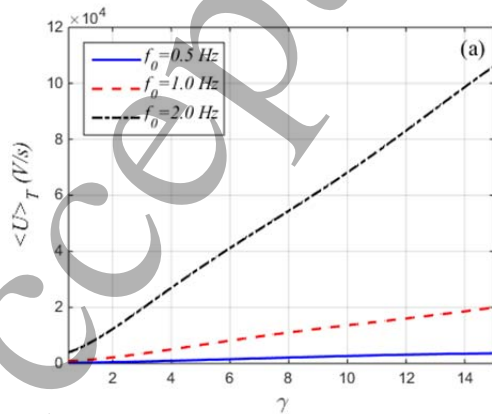
Figure 16. Output performance of the proposed device as a function of (a) amplitude and (b) frequency of the harmonic excitation, $r=1$.

5.2. System output under disturbed harmonic excitation

In real world, a pure harmonic excitation is easily disturbed due to various factors. For example, in many applications, like human walking straight, up and down or jogging, it is impossible to maintain a constant frequency and the phase of harmonic excitation may be modulated randomly. In this case, the system external excitation is $F(t) = A\cos(2\pi f_0 t + \sigma\xi(t))$, where $\xi(t)$ is Gaussian white noise with zero-mean and unit-variant, and $D=\sigma^2$ represents its intensity.

Let $\gamma=5$, $f_0 = 2$ Hz and σ varies from 0 to 10, then the numerically obtained curve of $\langle U \rangle_T$ versus D is plotted in Figure 17. This curve is fitted to approximate numerical results where each blue cross expresses the result of averaging over 100 samples. As expected, the maximum amount of energy is harvested when the system is under pure harmonic excitation or tuned. With an increase in the noise intensity the system becomes out of tune and the amount of harvested energy drops significantly, which can be seen in Figure 17. Increasing the noise intensity further will make the harmonic signal looks like a bounded noise but relatively large value of γ allows the ball to impact the membranes almost all the time, thus at values of noise intensity between 10 and 100 the amount of $\langle U \rangle_T$ stays almost the same. Two smaller plots shows the voltage pattern at value of $D=1$ and $D=81$. The latter has visible lower number of impacts, which are significantly weaker.
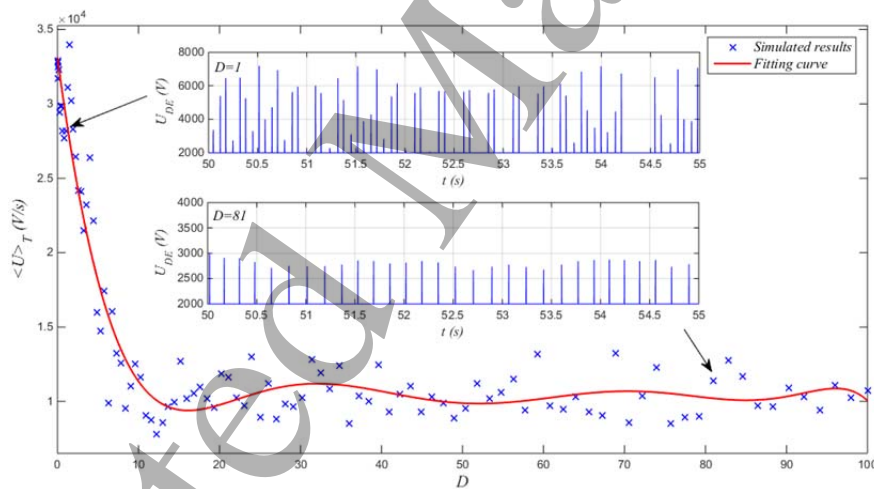

Figure 17. Output performance of the proposed device under phase modulations and two responses at low and high intensity ranges. $r=1$ and zero initial conditions were chosen.

5.3. Comparison to an EMEH "shaking" flashlight system

In order to better evaluate the output performance of the proposed device, an electromagnetic (EM) energy harvesting system [35] is used to compare with our device. The curved EM system, which has a similar shape with the device proposed in this paper, consists of a cylinder and a magnet moving freely inside. It is able to capture energy through oscillatory motion and proposed the use of a curved oscillatory electromagnetic harvester over the regular linear EM harvester. The largest power density of this curved EM system was 0.123 mW/cm^3 among the vibrational frequency range 2-5 Hz.

For the comparison under a same size, the dimensions of the devices and the ball proposed in this paper were taken the same as the dimensions of the curved EM system, and other characteristics were taken as following: $r = 0.5$, $R_{in} = 8$ mm, $r_b = 7.5$ mm, M=0.012 Kg, $m = 0.053$ Kg, $\varepsilon_0 = 8.85 \times 10^{-12}$ F/m, $\varepsilon_r = 3.4$, $C = \varepsilon_0 \varepsilon \pi R_{in}^2 / h_1 = 2.42 \times 10^{-11}$ F, V=42.2 cm^3. The output power of the proposed device under these parameters is estimated according to (14) in Table 3, where the power density is also presented. It can be seen that the power densities of the proposed device are much larger than that of the curved EM system at the given frequency range, which indicates the superiority of the proposed device compared with a shape-similar EM vibrational energy harvesting system. What should be noted is that, the power density of the proposed system has a positive relationship with the value of U_{in} according to (14), which provides a flexibility for the proposed system to produce a higher power density by increasing the value of U_{in}.

Table 3. The comparison of power density between the proposed device and the Curved EM system.

	Input data			Output power	Power density
Proposed device	$f_0 = 2$ Hz	A=5 N	$U_{in} = 2000$ V	0.061 W	1.447 mW/cm^3
Proposed device	$f_0 = 5$ Hz	A=5 N	$U_{in} = 2000$ V	0.132 W	3.128 mW/cm^3
Curved EM system [35]	$f_0 = 2-5$ Hz	N/A	N/A	0.005 W	0.123 mW/cm^3

According to the analyses and discussion in this subsection, one can find that the energy converted by the proposed system from periodic vibration is significantly affected by its intensity. The frequency of the periodic vibration also has a positive affection in the system output. The phase modulations of the excitation have a negative influence on the energy harvesting in general. It can be inferred that provided the intensity of the vibration is large, even those periodic vibration with low frequency can be converted to electrical energy. This is a major advantage of the proposed DE-based energy harvesting system because it potentially allows utilizing the device for harnessing vibrational energy from sources of energy with not perfectly period excitation like human waking or wind. Another superiority of the proposed device is that the power intensity can also be enhanced by increasing the input voltage.

6. Conclusion

In this paper a DE-based energy harvesting device has been proposed and analyzed. The concept is based on the vibro-impact motion of a ball, moving freely inside a capsule (cylinder) with both sides of it covered by DE membranes and excited externally. First, mechanical properties of the DE membranes were studied experimentally to identify their stiffness properties by generating force vs. displacement curve. This nonlinear relationship has been used in the vibroimpact model of the DE EH device to calculate the deformation of the membrane. The membrane deformation was analytically connected to the amount of voltage that can be generated from the DE membrane, which behaves as a variable capacitor. Numerical simulations for pure harmonic excitation have shown colourful variety of ball responses depending on initial conditions, amplitude and frequency of the excitation. Several cases have been studied, including a saw-tooth response, and normalized amount of gained voltage has been obtained. Curves of output voltage gain over time as a function of the excitation amplitude

or frequency have shown increasing trends, indicating an increase in the gained power. It should be stressed that the amounts observed in the studied cases have a similar magnitude at $r = 2$ Hz and $r = 1$. Another interesting fact is the amounts of gained voltage in the system with inelastic impacts ($r = 0.6$ and $r = 0.3$) are larger than that in the system with $r = 1$. Numerical results for the disturbed harmonic excitation resulted in decrease of the output voltage gain, which can be explained by out of tune action of the external excitation. At last, the comparison study has been conducted with an electromagnetic energy harvesting system, which has a similar shape with the proposed device. The comparison results validate the potential superiority of the proposed system.

Acknowledgments

References

[1] Gao Y J, Leng Y G, Fan S B and Lai Z H 2014 *Smart Mater. Struct.* **23** 095003
[2] Leng Y G, Gao Y J, Tan D, Fan S B and Lai Z H 2015 *J. Appl. Phys.* **117** 064901
[3] Gao Y, Leng Y, Javey A, Tan D, Liu J, Fan S and Lai Z 2016 *Smart Mater. Struct.* **25** 115032
[4] Beeby S P, Tudor M J and White N M 2006 *Meas. Sci. Technol.* **17** R175
[5] Kang G, Kim K S and Kim S 2011 *Rev. Sci. Instrum.* **82** 046101
[6] Mckay T G, Rosset S, Anderson I A and Shea H 2014 *Smart Mater. Struct.* **24** 015014
[7] Li T, Qu S and Yang W 2012 *J. Appl. Phys.* **112** 034119
[8] Bortot E and Gei M 2015 *Extreme Mechanics Letters* **5** 62-73
[9] Huang J, Shian S, Suo Z and Clarke D R 2013 *Adv. Funct. Mater.* **23** 5056-5061
[10] McKay T G, O'Brien B M, Calius E P, Anderson I A 2011 *Appl. Phys. Lett.* **98** 142903
[11] Jean-Mistral C, Vu Cong T and Sylvestre A 2012 *Appl. Phys. Lett.* **101** 162901
[12] Lv X, Liu L, Liu Y and Leng J 2015 *Smart Mater. Struct.* **24** 115036
[13] Pelrine R, Kornbluh R D, Eckerle J, Jeuck P, Oh S, Pei Q and Stanford S 2001 *SPIE's 8th Annual International Symposium on Smart Structures and Materials* vol 4329 148-156
[14] Suo Z, Zhao X and Greene W H 2008 *J. Mech. Physics of. Solids* **56** 467-486
[15] Schmidt A, Rothemund P and Mazza E 2012 *Sensors Actuat A-Phys.* **174** 133-138
[16] Koh S J A, Keplinger C, Li T and Bauer S 2011 *IEEE/ASME T. Mech.* **16** 33-41
[17] Tröls A, Kogler A, Baumgartner R, Kaltsels R, Keplinger C, Schwödiauer R, Graz I and Bauer S 2013 *Smart Mater. Struct.* 22 104012
[18] Zhu Y, Wang H, Zhao D and Zhao J 2011 *Smart Mater. Struct.* **20** 115022
[19] Graf C, Hitzbleck J, Feller T, Clauerg K, Wagner J, Krause J and Maas J 2014 *J. Intel. Mat. Syst. Str.* **25** 951-966
[20] Chiba S, Waki M, Wada T, Hirakawa Y, Masuda K and Ikoma T 2013 *Appl. Energ.* **104** 497-502
[21] Moretti G, Forehand D, Vertechy R, Fontana M and Ingram D 2014 *ASME 2014 33rd International Conference on Ocean, Offshore and Arctic Engineering* OMAE2014-23559
[22] Vertechy R, Fontana M, Papini G P R and Forehand D 2014 *SPIE Smart Structures and Materials, Nondestructive Evaluation and Health Monitoring* vol 9056 90561G
[23] Koh S J A, Zhao X and Suo Z 2009 *Appl. Phys. Lett.* **94** 262902
[24] Ibrahim R A 2009 *Vibro-impact dynamics: modeling, mapping and applications* (Springer Science & Business Media)
[25] Dimentberg M F and Iourtchenko D V 2004 *Nonlinear Dynam.* **36** 229-254
[26] Iourtchenko D V and Song L L 2006 *Int. J. Nonlin. Mech* **41** 447-455
[27] Moss S, Powlesland I, Galea S and Carman G 2010 *SPIE Smart Structures and Materials+ Nondestructive Evaluation and Health Monitoring* 76431
[28] Jacquelin E, Adhikari S and Friswell M I 2011 *Smart Mater. Struct.* **20** 105008

[29] Halim M A, Khym S and Park J Y 2013 *J. Appl. Phys.* **114** 044902

[30] Moss S, Barry A, Powlesland I, Galea, S, and Carman, G. P A 2010 *Appl. Phys. Lett.* **97** 234101

[31] Mak K H, McWilliam S, Popov A A, and Fox C H J 2011 *Structural Dynamics and Renewable Energy* vol 1 273-280 (Springer New York)

[32] Borowiec M, Litak G and Lenci S 2014 *International Journal of Structural Stability and Dynamics* **14** 1440020

[33] Gendelman O V and Alloni A 2015 *J. Sound Vib.* **358** 301-314

[34] Truong B D, Le C P and Halvorsen E 2015 *28th IEEE International Conference on Micro Electro Mechanical Systems (MEMS)* 1125-1128.

[35] Samad F A, Karim M F, Paulose V, Ong L C. 2016 *IEEE Sensors Journal* **16** 1969-1974.